Lattice Disorder and Size-Induced Kondo Behavior in $CeAl_2$ and $CePt_{2+x}$

S.-W. Han,[1,2] C. H. Booth,[1] E. D. Bauer,[3] P. H. Huang,[4] Y. Y. Chen,[4] and J. M. Lawrence[5]

[1]*Chemical Sciences Division, Lawrence Berkeley National Laboratory, Berkeley, California 94720, USA*
[2]*Chonbuk National University, Jeonju, 561-756, Korea*
[3]*Los Alamos National Laboratory, Los Alamos, New Mexico 87545, USA*
[4]*Institute of Physics, Academia Sinica, Taipei, Taiwan, Republic of China*
[5]*Department of Physics, University of California, Irvine, California 92697, USA*

(Received 23 March 2006; published 31 August 2006)

When the size of $CeAl_2$ and $CePt_{2+x}$ particles is reduced to the nanometer scale, antiferromagnetism is suppressed and Kondo behavior predominates, with the Kondo temperature T_K either decreasing ($CeAl_2$) or increasing ($CePt_{2+x}$) relative to the bulk. Local structure measurements show that these nanoparticles are significantly distorted. While such distortions should strongly affect magnetic and electronic properties, we find they cannot explain the observed changes in T_K. Other size-induced changes to the electronic structure must, therefore, play a significant role.

DOI: 10.1103/PhysRevLett.97.097204 PACS numbers: 75.20.Hr, 61.10.Ht, 61.46.−w, 71.23.−k

Despite recent interest in fundamental processes at the nanoscale, few studies of the effect of decreasing particle size on strongly correlated electron materials exist [1–3]. A recent exception involves the cerium-based Laves phase compounds $CeAl_2$ and $CePt_2$ which display the fascinating property that as their particle size becomes comparable to the nanometer scale, they change from displaying Kondo behavior above an antiferromagnetic (AF) transition [$T_N = 3.9$ K [4] and 1.6 K [5], respectively] to displaying only a nonmagnetic, Kondo ground state [6,7]. In addition, changes to the Kondo temperature T_K occur that are partially attributed to size effects [6]. However, an important component to the Kondo interaction is the f electron or conduction electron hybridization, which is a local effect that depends strongly on the local structural environment around the f ions. Therefore, lattice distortions or disorder could play an important role compared to particle size in determining interaction strengths and even whether or not the ground state is magnetic.

To clarify the structural issues, we report extended x-ray absorption fine structure (EXAFS) measurements on bulk and nanoparticle samples of $CeAl_2$, $CePt_2$ and $CePt_{2.5}$ [nonmagnetic, $T_K \approx 2$ K [5]] at the Ce and Pt L_{III} edges. These data indicate that large distortions exist in each of the nanophase materials. By using a tight-binding form for the hybridization matrix element V_{fc}, we demonstrate that, although these distortions are important, other size and surface-induced effects must also play a large role.

The nanoparticles are prepared by an evaporation method [6]. The average particle sizes and distribution widths are 8.0 ± 0.5 nm for $CeAl_2$ [6], 3.8 ± 0.3 nm for $CePt_2$, and 4.2 ± 0.3 for $CePt_{2.5}$ [7], as determined by high-resolution transmission electron microscopy (TEM). While the volume of $CeAl_2$ expands by 1.1% relative to the bulk [6], the $CePt_{2+x}$ nanoparticles *contract* by 6%. Estimates of T_K from the electronic coefficient $\gamma = C_{\mathrm{el}}/T$ to the linear part of the specific heat are hampered by the nearby AF ordering, but are estimated to be ~5 K for $CeAl_2$ [4] and 1–2 K for $CePt_{2+x}$ [5]. The nanoparticles display no AF, but do display changed $\gamma's$: the value $\gamma = 9\ \mathrm{J\,mol^{-1}\,K^{-2}}$ ($T_K = 0.5$ K) for nanoparticle $CeAl_2$ is among the largest measured for any compound [6]. In contrast, $\gamma \approx 20$–$40\ \mathrm{mJ\,mol^{-1}\,K^{-2}}$ ($T_K \approx 700$ K assuming $J = 5/2$) for these $CePt_{2+x}$ nanoparticles [7].

The bulk samples were ground for x-ray absorption measurements and passed through a 20 μm sieve. All powders were brushed onto adhesive tape and stacked to obtain samples with absorption edge steps corresponding to 0.3–1.0 absorption lengths. Transmission Ce and Pt L_{III}-edge spectra on $CeAl_2$ and $CePt_{2.5}$ were obtained on BL 2–3 at the Stanford Synchrotron Radiation Laboratory (SSRL) using a half-tuned Si(111) double-crystal monochromator. Data were collected on $CePt_2$ at the Pacific Northwest Corsortium-Collaborative Access Team of the Advanced Photon Source (APS) using a 3/4-tuned Si(111) double-crystal monochromator.

Ce L_{III}-edge x-ray absorption near-edge structure (XANES) results are displayed in Fig. 1, after a preedge background subtraction. XANES measurements are widely used for determining cerium valence [for instance, see Ref. [3]]. These data show a dramatic change between the bulk and nanoparticle samples, with the main peak near 5725 eV noticeably sharper in the nanoparticle spectra. A new peak appears in the nanoparticle $CePt_{2+x}$ spectra near 5735 eV, indicative of a shift toward tetravalence. Fits using a combination of arctangents and pseudo-Voigts give the f-electron occupancy n_f. This procedure has been shown to be accurate within ~5% [3]. Note that the nanoparticle values reported in Fig. 1 include the contribution of a small CeO_2 impurity as discussed below. Adjusting these measurements to account for this impurity only increases n_f by about 0.06 in the nanoparticle component. Another interesting point is the observed shift in energy of the leading peak in the $CePt_{2+x}$ nanoparticle data. Such shifts occur in systems where a ligand hole develops coupled to a trivalent cerium configuration,

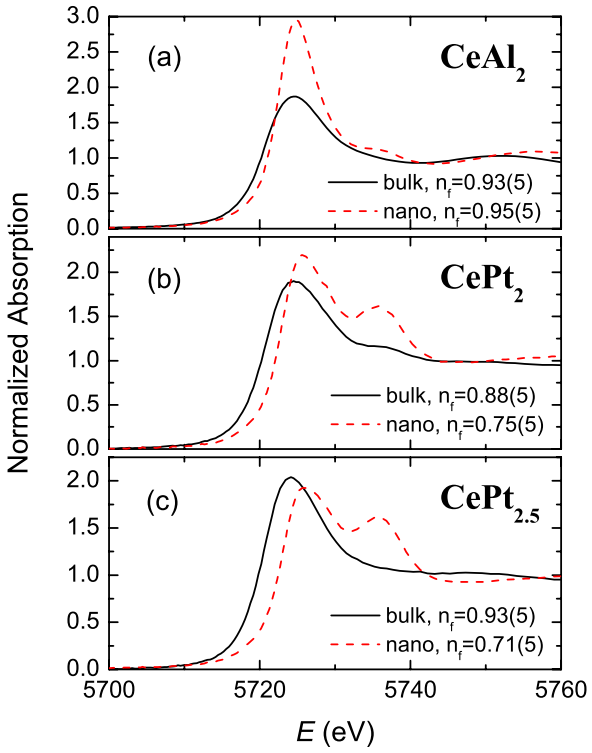

FIG. 1 (color online). Ce L_{III}-edge XANES at 20 K on (a) $CeAl_2$, (b) $CePt_2$, and (c) $CePt_{2.5}$, together with estimates of n_f. These n_f estimates include the contribution of any cerium impurities (see text). Energy is calibrated by setting the first inflection point of the CeO_2 Ce L_{III} edge to 5724.0 eV.

such as in CeO_2, and have also been observed in other mixed-valent cerium systems with bonding intermediate between metallic and covalent [3].

These data therefore show that Ce in $CeAl_2$ remains close to trivalent, consistent with the high value of γ, while the strongly mixed-valent character of the $CePt_{2+x}$ nanoparticles is known to correlate with large Kondo temperatures, $T_K > 100$ K [8]. Together with the observed decreases in the specific heat, we conclude the $CePt_{2+x}$ nanoparticles have a high $T_K \approx 700$ K.

EXAFS data were analyzed with the UWXAFS package [9] using standard procedures [10] and photoelectron backscattering functions calculated with the FEFF8 code [11]. After the atomic background absorption μ_0 was determined, the EXAFS function $\chi = \mu/\mu_0 - 1$ was obtained. Figure 2 shows the EXAFS for all three samples as a function of the photoelectron wave vector $k = \hbar^{-1}\sqrt{2m_e(E-E_0)}$, where m_e is the electron rest mass, E is the incident photon energy, and E_0 is the edge energy, chosen arbitrarily at the half height of the edge. The weak EXAFS oscillations from the nanoparticles indicate that their local structures are considerably disordered compared to their bulk counterparts.

Figure 3 shows the magnitude of the Fourier transformed (FT) EXAFS data from bulk and nanocrystalline samples of $CePt_2$. FT data for $CeAl_2$ [12] and $CePt_{2.5}$ are

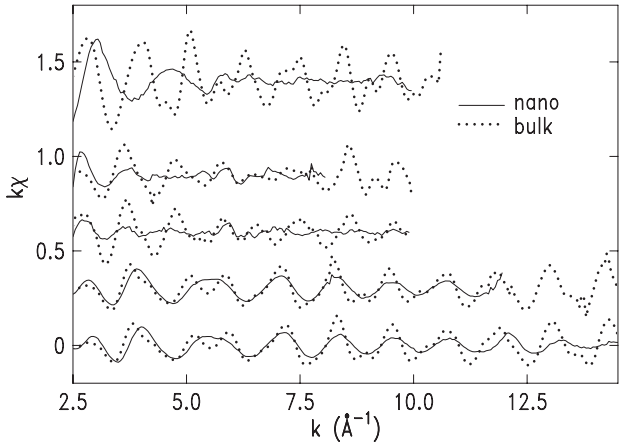

FIG. 2. EXAFS ($k\chi$) as a function of k measured at 20 K. From top, Ce L_{III} edge on $CeAl_2$, $CePt_2$ and $CePt_{2.5}$, and Pt L_{III} edge on $CePt_2$ and $CePt_{2.5}$. The Ce L_{III}-edge EXAFS data are limited to $k = 10$ Å^{-1} by the Ce L_{II} edge.

similar to the $CePt_2$ transforms. Note that peaks are shifted from their true pair distances due to the phase shift of the back scattered photoelectron. Detailed fits are therefore necessary to obtain quantitative information. Fits to the bulk data start from the $C15$ Laves structure (space group $F\bar{4}3m$). The immediate environment around the Ce atoms on the $4a$ and $4c$ sites consists of 12 Al or Pt nearest neighbors arranged in an irregular octahedron, closely followed by 4 Al or Pt atoms. The local environment around the Al and Pt atoms consists of 6 nearest-neighbor Al or Pt's followed by 6 Ce's at a somewhat longer dis-

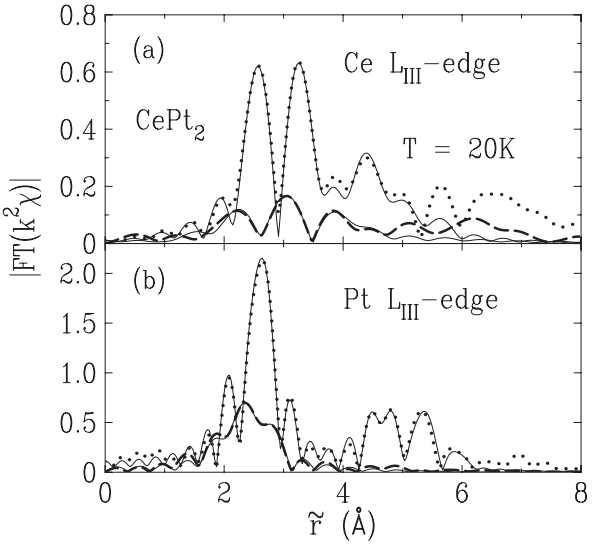

FIG. 3. FT magnitude of EXAFS data from bulk (dotted line) and a nanoparticle (thick-dashed line) samples of $CePt_2$ from (a) the Ce edge and (b) the Pt edge. Solid lines are best fits. Ce edge data are transformed from 2.7–7.5 Å^{-1} (nanoparticles) or 2.5–9.5 Å^{-1} (bulk). Pt data are transformed from 2.5–14.5 Å^{-1} (bulk) or 2.5–11.5 Å^{-1} (nanoparticles). All FT's use a Hanning window of width 0.5 Å^{-1}.

tance. Note that the $CePt_{2.5}$ sample nominally has Pt on 1/7th of the 4*a* and 4*c* sites. The amplitude fractions for all pairs are held fixed to the nominal values in the fits to the bulk data. The fit quality is high, and the number of fit parameters is well below the number of independent data points [13]. The fit results are summarized in Table I. The small σ^2's for bulk $CeAl_2$ (e.g., Ce-Al $\sigma^2 = 0.0038$ Å^2) indicate strong local order. The bulk σ^2's for the $CePt_{2+x}$ samples indicate some disorder exists even in the starting material (e.g., Ce-Pt in $CePt_2$ $\sigma^2 = 0.012$ Å^2). In any case, the measured local pair distances agree well with the average structures derived from diffraction measurements [5,14].

The nanoparticle fit results are more complex. Reliable results are not obtained for the Ce-Ce or more distant shells in $CeAl_2$ nanoparticles. CeO_2 contamination is expected [6], and in fact the fit is considerably improved by including 1.2 ± 0.6 oxygens at ~2.44 Å, along with the main Ce-Al pairs at 2.96 Å. The Ce-O amplitude is consistent with ~15% CeO_2 (all percentages are atomic %, where applicable), in agreement with Ref. [6], although the bond length is somewhat larger than the bulk CeO_2 value of 2.34 Å [15]. The situation is similar for the $CePt_{2+x}$ nanoparticles. The fits are not sensitive to Pt-O contamination or Ce-O in further shells within ~20%, or to Ce/Pt site interchange beyond the nominal concentrations within ~12%. X-ray diffraction and TEM estimates of the oxide concentration ~5% [6] agree that for bulk CeO_2 contamination, these EXAFS estimates are likely high. However, an amorphous CeO_2 component could exist at the ~15% level, possibly from a surface contribution on the intermetallic nanoparticles.

In any case, the average σ^2 of the Ce-Al and Ce-Pt pairs is much larger and their pair distances are considerably shorter than that of the same pairs in the bulk samples. Ce-Ce pairs in the $CePt_{2+x}$ samples show a somewhat smaller contraction than the Ce-Pt pairs, but also show a large amount of disorder in the nanoparticles. Note that the same Ce-Pt pair distance is measured from the Pt L_{III} edge. Also note that the number of neighbors in the nanoparticles is similar to the bulk value, although the error bars are large beyond the nearest neighbors.

While these measurements indicate that both large distortions and intrinsic disorder exist around Ce in the nanoparticles, the local structure is still describable as a Laves phase. Interestingly, the Pt-Pt pairs, which are about the same distance apart as in elemental Pt [15], contract only slightly compared to those in the bulk $CePt_{2+x}$ samples. This contraction is nearly equal to that expected from the change in the cell volume, so the Pt's (and by analogy, the Al's) likely determine the lattice constant. This rigidity indicates that the Pt octahedrons around the Ce's remain about the same size in the nanoparticles. Since the Ce-Pt pairs have strongly contracted, the Ce atoms must be off center in the Pt octahedrons. A similar argument holds for the $CeAl_2$ nanoparticles. In this case, the measured pair distance would be dominated by the shortest atom pairs and a large static component to σ^2 would develop, consistent with the observations. An analysis [16] including a skewed pair-distance distribution was, however, inconclusive.

Although the microscopic nature of the distortions remains unclear, further details can be inferred. For instance, it is possible that Ce distorts everywhere within a given nanoparticle in the same way. However, a more likely scenario is that some surface reconstruction occurs with Ce migrating toward the surface. Any oxide layer would have the same effect. It is important to note that for a spherical ~8 nm particle like the $CeAl_2$ particles, about 25% of the atoms lie within 4 Å of the surface, while for ~4 nm, $CePt_{2+x}$ particles, about 50% of the atoms lie within a similar layer. If a cerium migration or oxidation takes place within this layer, a distribution of distortions within a single nanoparticle will develop. One then expects

TABLE I. Fit results at 20 K. A single value of S_0^2 and ΔE_0 was used for each sample at each edge. S_0^2 was determined from the bulk sample by fixing the number of neighbors N to the nominal values, and then used for the nanoparticle data.

			Bulk sample			Nanoparticle sample		
	pair	S_0^2	N	r(Å)	σ^2(Å^2)	N	r(Å)	σ^2(Å^2)
$CeAl_2$	Ce-Al	0.90(6)	12	3.356(5)	0.0038(4)	11(2)	2.96(2)	0.044(9)
	Ce-Ce		4	3.503(6)	0.0021(7)			
	Ce-O					1.2(6)	2.44(3)	0.006(4)
$CePt_2$	Ce-Pt	0.85(10)	12	3.18(1)	0.012(1)	11(1)	2.91(1)	0.025(7)
	Ce-Ce		4	3.43(1)	0.002(1)	3.8(6)	3.37(1)	0.017(5)
	Ce-O					1.5(6)	2.50(5)	0.025(9)
	Pt-Pt	0.83(5)	6	2.723(2)	0.0015(2)	6.4(5)	2.690(5)	0.0051(2)
	Pt-Ce		6	3.19(1)	0.013(1)	6(1)	2.86(2)	0.048(8)
$CePt_{2.5}$	Ce-Pt	0.95(10)	12	3.18(1)	0.014(1)	10.8(10)	2.84(1)	0.021(1)
	Ce-Ce/Pt[a]		4	3.44(2)	0.003(1)	3.9(5)	3.29(1)	0.024(2)
	Ce-O					1.6(3)	2.39(3)	0.020(6)
	Pt-Pt	0.85(7)	5.6	2.713(2)	0.0019(2)	6.1(6)	2.690(3)	0.0056(3)
	Pt-Ce/Pt[a]		5.87	3.13(1)	0.014(1)	5.5(9)	2.92(3)	0.034(5)

[a]6/7th of N are Ce, 1/7th are Pt, R constrained to the same value, σ^2's constrained by the ratio of the reduced masses.

different distortions or oxide-layer contributions corresponding to different particle sizes. All of these scenarios should occur at some level, and will have important consequences for the magnetic interactions.

Although modeling all these effects would ideally use a real many-body calculation, much can be learned by considering the Kondo interactions in the simple form $T_K = W\exp[-\epsilon_f/(\rho V_{fc}^2)]$. Both the conduction bandwidth W and the density of states at the Fermi level ρ depend on long-range effects and are difficult to predict in the nanophase. V_{fc}, however, is dominated by local interactions, so a tight-binding model [17] can be employed. The f-level energy ϵ_f should not change much between the bulk and nanophase material. Using this model, we assign to V_{fc} changes in T_K that are due only to the structural distortions. Particle-size effects are then described by changes in W and ρ. We can then test whether particle-size effects are important in these materials by fixing W and ρ/ϵ_f based on the measurement of T_K in the bulk sample, and then comparing the expected change in T_K due to changes in V_{fc} to the measured nanoparticle T_K's. The relevant tight-binding form for V_{fc} is

$$V_{ll'} = \sum_{\text{pairs}} \frac{\eta_{ll'}\hbar^2}{m_e} \frac{\sqrt{r_l^{2l+1} r_{l'}^{2l'+1}}}{R_{ll'}^{l+l'+1}}, \qquad (1)$$

where l and l' are the angular momentum quantum numbers of the f and the conducting electronic shells, r_l's are the effective shell radii [tabulated in Ref. [17]], and $R_{ll'}^{l+l'+1}$ is the distance between the l ion and the l' ion. The constant $\eta_{ll'}$ is (assuming σ bonds) $\eta_{fp} = 14.6$ and $\eta_{fd} = 141.2$ for the cases given here [17].

Ignoring changes in sign and using these equations with the bulk $CeAl_2$ crystal structure, $V_{fp}(\text{bulk}) = 1.81$ eV. If we assume $W = 1$ eV and $T_K = 5$ K, then $\epsilon_f/\rho = 25.4$ eV^2. Using the lattice constants for the nanoparticle, but assuming no other distortions, gives $V_{fp}(\text{nano}) = 1.78$ eV, and with the above values of W and ϵ_f/ρ, $T_K = 3.8$ K. As noted by Chen *et al.* [6] using a different scaling argument, this value is still ~5 times larger than the observed value, and they ascribe the difference to surface or size effects. These effects would presumably be manifest as a decrease in either ρ and/or W in the nanoparticle, either of which seem likely. This analysis is not qualitatively affected by assuming a very different W.

Disorder can generate a distribution of Kondo temperatures [18], and hence local structure distortions should be included when evaluating Eq. (1). This sum shows that distortions consistent with our measurement give on average an even larger hybridization than in the ordered bulk sample, implying a higher, not lower, T_K. Any surface oxidation also would give an effectively higher T_K. This analysis places most of the burden for decreasing T_K on the longer-range, size-induced effects of W and ρ.

The situation in reversed for the $CePt_{2+x}$ samples, since T_K is observed to increase in the nanoparticle to greater than 100 K relative to the bulk material ($T_K \approx 1$ K). Using a similar procedure as above and the measured lattice constants for both bulk and nanoparticle $CePt_2$ samples, V_{fd} should increase from 1.86 eV in the bulk to 2.11 eV in the nanoparticle, corresponding to a T_K of 8 K. Including the measured distortions nearly doubles this estimate of T_K, which is not enough to explain the observed strong mixed valence in Fig. 1. A dramatic increase in ρ or W is likely necessary, such has been observed in vanadium nanoparticles [19]. However, given the increased surface to volume ratio in these particles, a surface oxidation may also be important.

In summary, while cerium in $CeAl_2$ remains close to trivalent in the nanoparticle, a strong shift toward mixed valence occurs in the $CePt_{2+x}$ nanoparticles. In addition, a substantial off-center distortion of the Ce atoms in the nanoparticles is observed. Despite the magnitude of this distortion, we find that it cannot explain either the sign or the magnitude of the observed changes in the electronic specific heat, demonstrating that long-range effects such as the conduction bandwidth and the density of states at the Fermi level are in direct competition with the structural distortions. These effects create a complicated landscape for exploring Kondo interactions under the influence of size and disorder effects.

This work was supported by the Office of Science, U.S. Department of Energy (DOE) under Contract No. DE-AC02-05CH11231. Data were collected at the SSRL and at the APS, both national user facilities supported by the US DOE and Office of Basic Energy Sciences.

[1] W. B. Thimm *et al.*, Phys. Rev. Lett. **82**, 2143 (1999).
[2] P. Schlottmann, Phys. Rev. B **65**, 024431 (2001).
[3] C. H. Booth *et al.*, Phys. Rev. Lett. **95**, 267202 (2005).
[4] F. Steglich *et al.*, J. Phys. (Paris), Colloq. **40**, C5-301 (1979), and references therein.
[5] J. M. Lawrence *et al.*, Phys. Rev. B **56**, 5 (1997).
[6] Y. Y. Chen *et al.*, Phys. Rev. Lett. **84**, 4990 (2000).
[7] Further details of the $CePt_{2+x}$ properties will be the subject of a future paper.
[8] N. E. Bickers *et al.*, Phys. Rev. B **36**, 2036 (1987).
[9] E. A. Stern *et al.*, Physica (Amsterdam) **208-209B**, 117 (1995); see also http://depts.washington.edu/uwxafs.
[10] S.-W. Han *et al.*, Phys. Rev. B **66**, 094101 (2002).
[11] A. L. Ankudinov *et al.*, Phys. Rev. B **58**, 7565 (1998).
[12] S.-W. Han *et al.*, J. Magn. Magn. Mater. **272–276**, E101 (2004).
[13] E. A. Stern, Phys. Rev. B **48**, 9825 (1993).
[14] W. H. Zachariasen, Acta Crystallogr. **2**, 388 (1949).
[15] R. W. G. Wyckoff, *Crystal Structures* (Interscience Publishers, New York, 1964), 2nd ed.
[16] P. Eisenberger and G. S. Brown, Solid State Commun. **29**, 481 (1979).
[17] W. A. Harrison, in *Elementary Electronic Structure* (World Scientific, Singapore, 1999), p. 644.
[18] C. H. Booth *et al.*, Phys. Rev. B **66**, 140402(R) (2002).
[19] O. Vergara *et al.*, J. Phys. Chem. Solids **45**, 251 (1984).